NeuroImage 125 (2016) 880–894

Contents lists available at ScienceDirect

NeuroImage

journal homepage: www.elsevier.com/locate/ynimg

Carbon-wire loop based artifact correction outperforms post-processing EEG/fMRI corrections—A validation of a real-time simultaneous EEG/fMRI correction method

Johan N. van der Meer [a,b,c,h,*], André Pampel [d], Eus J.W. Van Someren [e,g], Jennifer R. Ramautar [e], Ysbrand D. van der Werf [f,g,h], German Gomez-Herrero [e], Jöran Lepsien [d], Lydia Hellrung [i], Hermann Hinrichs [c], Harald E. Möller [d], Martin Walter [a,b,j,*]

[a] Clinical Affective Neuroimaging Laboratory, Otto-von-Guericke University, Magdeburg, Germany
[b] Department of Behavioral Neurology, Leibniz Institute for Neurobiology, Magdeburg, Germany
[c] Department of Neurology, Otto-von-Guericke University, Magdeburg, Germany
[d] Max Planck Institute for Human Cognitive and Brain Sciences, Leipzig, Germany
[e] Department of Sleep and Cognition, Netherlands Institute for Neuroscience, An Institute of the Royal Academy of Arts and Sciences, Amsterdam, Netherlands
[f] Department of Cognition and Emotion, Netherlands Institute for Neuroscience, An Institute of the Royal Academy of Arts and Sciences, Amsterdam, Netherlands
[g] Department of Integrative Neurophysiology, Center for Neurogenomics and Cognitive Research (CNCR), Neuroscience Campus Amsterdam, VU University and Medical Center, Amsterdam, The Netherlands
[h] Department of Medical Psychology, Center for Neurogenomics and Cognitive Research (CNCR), Neuroscience Campus Amsterdam, VU University and Medical Center, Amsterdam, The Netherlands
[i] Department of Psychiatry and Neuroimaging Center, Technische Universität Dresden, Dresden, Germany
[j] Department of Psychiatry, Otto-von-Guericke University, Magdeburg, Germany

ARTICLE INFO

Article history:
Received 11 February 2015
Accepted 2 October 2015
Available online 24 October 2015

ABSTRACT

Simultaneous EEG-fMRI combines two powerful neuroimaging techniques, but the EEG signal suffers from severe artifacts in the MRI environment that are difficult to remove. These are the MR scanning artifact and the blood-pulsation artifact — strategies to remove them are a topic of ongoing research. Additionally large, unsystematic artifacts are produced across the full frequency spectrum by the magnet's helium pump (and ventilator) systems which are notoriously hard to remove. As a consequence, experimenters routinely deactivate the helium pump during simultaneous EEG-fMRI acquisitions which potentially risks damaging the MRI system and necessitates more frequent and expensive helium refills.

We present a novel correction method addressing both helium pump and ballisto-cardiac (BCG) artifacts, consisting of carbon-wire loops (CWL) as additional sensors to accurately track unpredictable artifacts related to subtle movements in the scanner, and an EEGLAB plugin to perform artifact correction. We compare signal-to-noise metrics of EEG data, corrected with CWL and three conventional correction methods, for helium pump off and on measurements. Because the CWL setup records signals in real-time, it fits requirements of applications where immediate correction is necessary, such as neuro-feedback applications or stimulation time-locked to specific sleep oscillations. The comparison metrics in this paper relate to: (1) the EEG signal itself, (2) the "eyes open vs. eyes closed" effect, and (3) an assessment of how the artifact corrections impacts the ability to perform meaningful correlations between EEG alpha power and the BOLD signal.

Results show that the CWL correction corrects for He pump artifact and also produces EEG data more comparable to EEG obtained outside the magnet than conventional post-processing methods.

Introduction

The simultaneous combination of electroencephalography (EEG) and functional magnetic resonance imaging (fMRI) is valuable to non-invasively study human brain function, due to the complementary nature of the two acquired brain signals. In the last two decades, the combination has been used extensively to find brain regions correlated

* Corresponding authors at: Clinical Affective Neuroimaging Laboratory, Otto v. Guericke University, Leipziger Str. 44, D-39120 Magdeburg, Germany. Fax: +49 391 61 17 531.
E-mail addresses: johan.vandermeer@med.ovgu.de, johanvandermeer@gmail.com (J.N. van der Meer), martin.walter@med.ovgu.de (M. Walter).
URL's: http://www.canlab.de (J.N. van der Meer), http://www.canlab.de (M. Walter).

http://dx.doi.org/10.1016/j.neuroimage.2015.10.064
1053-8119/

with EEG patterns for epilepsy (Thornton et al., 2010; van Houdt et al., 2010, 2012), help the source reconstruction problem in EEG (Rosa et al., 2010), or gain insight in sources underlying fluctuations in the amplitude of spontaneous EEG oscillations (Chang et al., 2013; de Munck et al., 2009). A vast amount of effort is routinely put into the preprocessing of the EEG signal, since the MRI-related and the ballistocardiac artifacts (BCG) are very large relative to the EEG signal of interest (Debener et al., 2008). Moreover, any head motion (caused by talking, coughing, sneezing, motion of hands or feet etc) has to be avoided. In almost all reported cases, extremely advanced signal analysis pipeline have been utilized (Debener et al., 2007; Ritter et al., 2007) to deconvolve the acquired EEG and extract the signals of interest. Even then the topological distributions cannot always be trusted (Grouiller et al., 2007), or the time-frequency characteristics can still be unusable in certain frequency ranges (Zotev et al., 2011). Ideally, EEG parameters obtained during fMRI should be validated against those acquired outside the magnet room.

An issue concerning EEG/fMRI is that in order to minimize uncontrollable artifacts, the helium (He) pump is often switched off, because pump vibrations that are transmitted from the compressor unit of the pump to the scanner bore generate large artifacts on the EEG signal. These artifacts can occur in almost any frequency band, depending on the type of scanner (Nierhaus et al., 2013). Switching off the He pump is, however, not advised, as it limits the flow of He around the magnet's super-cooled elements. Switching off the He accelerates the wear on pump-system components, necessitates more costly refills of the cryostat and might increase the B0 field drift. As the He pump is designed for continuous operation, frequent switching may lead to malfunctions and, hence, an increased risk of a magnet quench. For this reason, switching off the He pump for the purpose of performing EEG/fMRI is not allowed at many sites. In laboratories where it is allowed, the duration the He pump is switched off is typically limited, which precludes long recordings or high throughput. We here focus on this often ignored issue and consider two different He pump systems in widely-used commercial MRI magnets.

A relatively recent development in EEG/fMRI is the use of reference signals in the artifact correction preprocessing pipeline for the correction of the BCG artifact (Chowdhury et al., 2014; Luo et al., 2014). One way for obtaining reference signals is the use of 'carbon-wire loops' (CWL) (Abbott et al., 2015; Masterton et al., 2007; Negishi et al., 2008). A major advantage is that they can be easily integrated into existing EEG/fMRI systems and do not require a new EEG electrode net to be constructed. By this add-on to the existing EEG cap, movement-induced signals can be measured as a result of Faraday's magnetic induction law. These signals could in turn assist in the removal of movement-induced artifacts in the EEG using simple regression. We hypothesize that the use of these reference signals will (1) give better artifact corrections than presently used methods addressing the BCG artifact, and will (2) additionally allow the removal of the He pump artifacts, since both artifacts originate from the movement of electrodes and electrode leads in the MRI magnet. Moreover, the reference signals may improve online correction, allowing for immediate monitoring of the EEG and real-time detection of EEG states or events.

An online correction, relying on actual scanner conditions without the need to have the complete data set, is especially important in real-time studies where detection of brain events in EEG is necessary. Furthermore, such detection places more stringent demands on the quality of the EEG signal than currently is possible with on-line correction methods. Any additional benefit above performance of existing post-processing methods is a likely prerequisite for real-time studies.

In the present paper, we introduce a straightforward way of implementing a complete CWL setup for the correction of the BCG and He pump artifacts for any EEG/fMRI system. Furthermore, we introduce a sliding window approach to use these CWL signals to regress out motion artifacts (both BCG and He pump artifact), which is published as a downloadable companion plug-in for EEGlab (Delorme and Makeig, 2004) (For obtaining the plugin via GitHub: https://github.com/jnvdmeer/CWRegrTool).

The novel CWL regression method will be compared against several current BCG artifact correction algorithms using simple 'eyes open-eyes closed' EEG experiments, at different scanners with different He pump systems. We will assess (1) the performance of the CWL regression approach to other commonly used methods, and (2) whether the CWL regression also removes He pump artifacts, allowing the use of EEG data acquired under 'He-pump on' conditions. In contrast to several recent approaches of EEG/fMRI that lack a comparison with EEG acquired in the absence of a strong magnetic field, we will directly test how the artifact-corrected EEG data relates to the signal quality of the EEG data recorded outside the magnet room.

Methods

Participants

Eight healthy volunteers (4 women), with a mean age of 25 years (range 20–30 years) participated in the experiment. Exclusion criteria were known contra-indications to MRI. All procedures were conducted in accordance with the Declaration of Helsinki and were approved by the Ethics Committee of the Faculty of Medicine of the University of Leipzig. Subjects gave informed written consent before participating in the study.

Experimental procedures

After participants were outfitted with the EEG cap, they performed a simple eyes open-eyes closed task three times; once outside of the magnet room and twice in one of two different scanners. Four subjects were scanned in a 3 T MAGNETOM TIM Trio (Siemens Healthcare, Erlangen, Germany) equipped with a conventional superconducting magnet (installed in 2003) and four other subjects in a 3 T MAGNETOM Verio scanner (Siemens Healthcare) equipped with a zero He-boil-off superconducting magnet (installed in 2010). The task consisted of five 'eyes open' blocks and four 'eyes closed' 30-second blocks within 4 min and 30 s, during which 136 functional scans were acquired. The screen presented the instructions to keep the eyes closed or open; 6 black/white 'flashes' helped the subject notice a change in condition when the eyes were closed. During the two assessments inside each scanner, the He pump was once on and once switched off.

Scanning was performed using equivalent 12-element head matrix coils on both scanners. The single-shot gradient-echo echo-planar imaging (EPI) sequence was equivalent for both scanners (echo time, TE, 30 ms; 192-mm field of view, 64×64 matrix, 3-mm slice thickness; 1-mm slice gap, 3×3 mm^2 nominal in-plane resolution, 30 axial slices aligned along the AC-PC line) except for the repetition time (TR 1.95 s on the TIM Trio and 2.00 s on the Verio). For each assessment, 136 functional scans were recorded. To enable accurate correction of MRI artifacts in simultaneously acquired EEG, the TR parameter of the EPI sequence was an exact multiple of the sampling interval of the EEG system (which is 0.2 ms with an EEG sampling rate of 5000 Hz). *For anatomical normalization*, *T_1-weighted* images were acquired using a three-dimensional magnetization-prepared rapid gradient echo (MP-RAGE) sequence (sagittal orientation) with selective water excitation and linear phase encoding (Mugler and Brookeman, 1990).

EEG signals from an MRI-compatible EEG cap of 32 channels were recorded using an MRI-compatible 'MR Plus' BrainAmp amplifier (Brain Products GmbH, Gilching, Germany) according to the 10–20 system. One additional electrode placed on the subject's upper back to record the ECG signal, and one electrode was attached close to the medial canthus of the left eye to measure the electro-oculogram (EOG). All electrodes were referenced to the FCz position with a ground electrode located at the AFz position. The impedance of all electrodes was maintained below 10 kΩ throughout the recording. The amplifiers were put

on a table just behind the rear end of the MRI scanner bore, 1 m away from the head coil. They were connected to a USB interface box and laptop inside the MR control room via optical cables going through the MR wave guide. A SyncBox device continually synchronized the amplifier clock (5000 Hz) to the MRI scanner clock (10 MHz). The amplifier's discriminative resolution was set to 0.5 μV/bit (range of +/− 16.38 mV). The signals were also hardware-filtered in the frequency band between 0.01 Hz and 250 Hz.

Carbon wire loops — hardware and regression

The CWL procedure has both a hardware component and a 'software' component. The hardware component (see Fig. 1A) consists of a set of carbon wires that detect motion-associated magnetic field changes (Masterton et al., 2007; Negishi et al., 2008). The software component performs the artifact correction within overlapping windows using a simple regression algorithm as described below.

Hardware

Our system consisted of four CWLs with an internal resistance of 160 Ω/m, sewn into the outer surface of an 32-channel EEG cap (Braincap MR, Brain Products, Gilching, Germany) at the left-frontal, left-posterior, right-frontal and right-posterior locations — in addition, two CWLs were attached to the cables going from the EEG cap to the EEG amplifier (BrainAmp MR Plus) (See Fig. 1A). The carbon wires consist of a 177 cm long double twisted strand of coated carbon-wire (CPVC4050, World Precision Instruments, Inc., Sarasota, FL, USA), with a loop of 10-cm diameter at the one side, and plugs suitable for the bipolar amplifier input box at the other side. The total resistance of one CWL is $177 \times 2 \times 160 = 566\ \Omega$. In the twisted part of the wire, induced

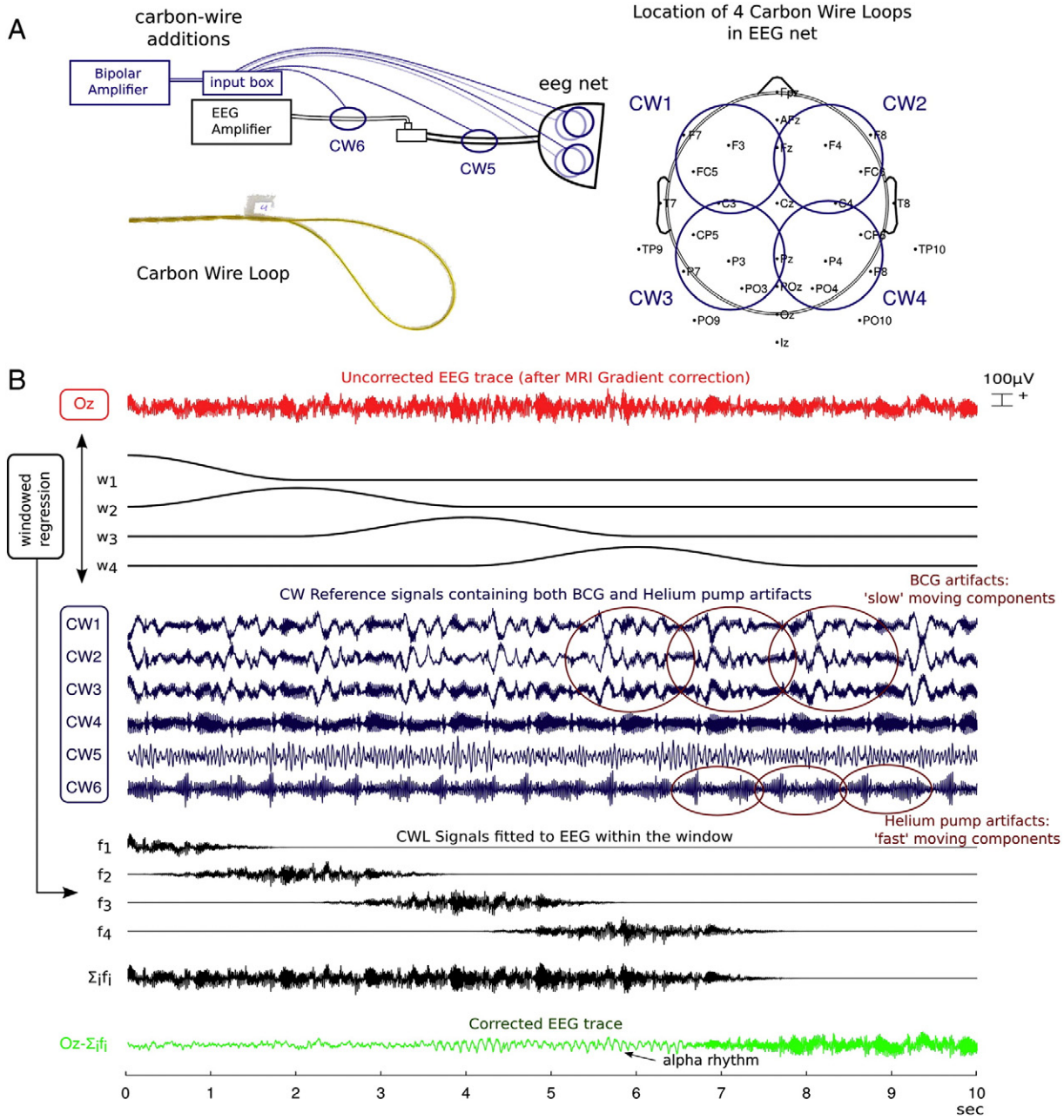

Fig. 1. (A): EEG cap equipped with Carbon-Wire Loops (4 on the net, 2 on the cables connecting the EEG cap to the amplifier). (B): Schematic illustrating the artifact correction. The signals from the 6 CWL's (in blue) are recorded simultaneously with the MR-corrected EEG data (in red). Windows are applied to both the 6 CWL's and the raw EEG signal and within the windows, the CWL signals are fitted to the EEG. The weighting of the windows allow them to be added such that their total weight equals 1 (black traces), creating a signal which is descriptive of the artifacts as informed by the CWL signals. Finally, the signal is simply subtracted to obtain cleaned EEG signal (in green).

signals are attenuated — only the loop itself picks up signals induced by motion, magnetic field gradients and radiofrequency (RF) pulses. The signals of the six CW loops are measured using an add-on in the form of a second BrainAmp ExG MR amplifier with an interface box. This is an MR-compatible amplifier able to measure bipolar inputs. The extra time needed to connect the carbon-wire loops to the ExG interface box, manage the extra cables, and place the extra (ExG) amplifier is about 2–3 min. In principle, any MR-compatible EEG system with the capability to measure bipolar signals would be able to have the CWL hardware incorporated.

Software

The software component implements a regression algorithm to simultaneously correct for any movement-related artifacts picked up by the CWLs as well as BCG, He pump and motion-related artifacts. It should be used after correction for MRI gradient artifacts with any method that takes advantage of the hardware synchronization of the EEG system with the MRI clock. In the current case, we chose the Bergen EEG-fMRI toolbox (Moosmann et al., 2009). After the MRI artifact removal, both the CWL signals and the EEG signals are band-pass filtered between 0.33 Hz to 125 Hz prior to the CWL regression. The removal procedure regresses out the motion-related artifacts using sliding Hanning windows with overlap between consecutive windows, as is shown in Fig. 1B. The Hanning windows can be set to any length (here 4 s — a trade-off between capturing at least some BCG artifacts and short-term adaptability of the regression). The windows overlap in such a way as to have an equally-weighted regression over the entire EEG trace. The Hanning-windowed approach prevents artificial 'jumps' in the EEG due to (rectangular) windowing (such as can be seen with the OBS approach in some cases). In addition, it allows the procedure to adapt to a new association between He pump and BCG artifacts as measured with the CWL and those present in the EEG trace due to small head posture changes. Finally, in contrast to AAS or OBS, the correction utilizes only information from within the current window — no other windows (taken from 10–20 s prior) are used to construct a template. This procedure alleviates constraints of motion-free windows to be included in the artifact correction algorithm.

Regression algorithm

Within the selected interval, the signal is extracted and multiplied by the Hanning window. Then, each CWL signal is shifted backwards and forwards in time, and each (time-shifted) regressor is added to the collection of regressors used in the regression (according to Eq. 1), so as to accommodate possible temporal delays between the waveform in the EEG and the waveform in the CWL signals. This is to accommodate that, unlike with the EEG signal itself (for which it can be safely assumed there is no *measurable* temporal delay between the time when the signal leaves the neuronal 'source' and arrives at the EEG 'sensor'), the CWL signals represent vibrations that are slower than the sampling rate of the EEG system. The BCG and He pump artifacts have different sources: for BCG it is the pulse wave and for Helium pump it is compressor unit of the coolant system. In both cases, they are waves that propagate throughout the entire EEG setup, including EEG cap, cables and amplifier. Because the CWL's are attached differently than the EEG electrodes, the motion of CWL and EEG sensors will occur with different time delays (the time delays are predominantly due to the BCG artifact). In addition, for each pair of CWL and EEG electrode, a vibration seen by the CWL should be transformed to approximate how this vibration is seen in the EEG — this transformation is associated with a transfer function. To take both the delay effect and the transformation into account, within any window, the regression is according to the following formula:

$$f(t_i)\sum_{k=-K}^{K}\sum_{j}\beta_{j,k}\mathrm{CW_j}(t_{i-k}) \quad (1)$$

The beginning and ending sample of the regressed part is given by:

$$(w1-) * \mathrm{fs} \le i \le w1 * \mathrm{fs} \quad (2)$$

where:

$\mathrm{fs} =$ amplifier sampling rate (Hz)

$w1 =$ window length (seconds)

$\mathrm{K} = 0.021 * \mathrm{fs}.$

In this work, we used a delay embedding of 21 ms to model for (i) the temporal delay between the artifacts captured with the CWL and the EEG, and (ii) the 'transfer function' between any CWL and EEG signal. See Supplementary Data (Section 1.4) for the rationale of this choice. This value of 21 ms should not be confused with the (much larger) value of 210 ms, which is associated with the delay between i) the R-peak of the QRS complex as seen in the ECG, and ii) the peak of the pulse artifact seen in the EEG (Allen et al, 1998).

In this way, each regression in the sliding window produces a windowed trace (see Fig. 1B). This represents the total fit of all six CWL signals to the EEG signal — and therefore represents all contributions to the EEG signal that can be attributed to motion — whether originating from the BCG pulse, the He pump, or head movement. When all windows in time are added together, it forms a continuous single trace that is simply subtracted from the uncorrected EEG trace, in order to produce an artifact-corrected EEG.

The regression is very fast and memory efficient. The most heavy computational step involves the inversion of a matrix (see Eq. 1); something which is required only once per window. On a standard dual-core 1.6 GHz laptop with 4G RAM, it takes about 15 s to correct a trace with 5 min of EEG data, 30 channels at a sampling frequency of 500 Hz.

MRI and EEG artifact correction(s)

The EEG data acquired simultaneously with the fMRI data were corrected for artifacts related to the gradient switching, following a previously published template subtraction procedure that takes into account head motions (Moosmann et al., 2009). For the averaging, to obtain an MRI template waveform, 25 MRI artifacts in a sliding window were used (Allen et al., 2000). This approach cannot optimally represent transitions, i.e. when abrupt changes of the artifact properties due to head movements occur. Therefore, a displacement vector is calculated from the motion parameters obtained from the realignment procedure of the imaging data, informing about head motions. Whenever this displacement vector reached a threshold value of 0.3, the window buffer was reset (Moosmann et al., 2009).

The displacement vector (d_j) was computed as follows:

$$d_i = sqrt\left(\Delta x_j^2 + \Delta y_j^2 + \Delta z_j^2\right) \quad (3)$$

where $\Delta x_j = x_j - x_{j-1}$, and x_j, y_j and z_j are framewise translation values, which is the output of motion correction of fMRI images. Use of the displacement vector and setting of a threshold value have been extensively tested and validated in a previous study (Moosman et al, 2009). Currently, there are MRI artifact correction algorithms published that use information of *all* MRI gradients artifacts to attenuate MRI noise that would likely perform better at MRI gradient removal, such as an approach with singular-value decomposition for generating MRI component waveforms (Liu et al., 2012) or an approach with clustering of MRI gradients into different sub-types (de Munck et al., 2013). However, we opted to use the Moosman method due to its availability as a freely downloadable plug-in for EEGlab, and the promise of its procedure to be used in a real-time artifact cleanup context.

Following MRI artifact correction, R-peak markers were placed in the ECG trace using BrainVision analyzer software. Missing misplaced and

double R-peak markers were controlled for. In order to achieve the best possible correction with AAS, OBS and OBS-ICA, this was followed with a visual inspection of the data. Data segments where the ECG channel was unclear (and no R-peak marker could be placed) or where the EEG data displayed motion artifacts that were unlike the BCG artifacts, were removed from the data and further analyses. Both R-peak markers and removed data segments were identical for all comparison between artifact corrections (including CWL). Data sets where R-peak detection is difficult due to bad quality of the ECG trace (Niazy, et al., 2005) could result in a sub-optimal EEG artifact correction. This could result in a relatively unfavorable comparison of AAS, OBS and OBS-ICA (which rely on accurate R-peak detection), with CWL (which does not require R-peak detection). Data sets where this occurred will be reported in the results section, and discussed accordingly.

The EEG data were further corrected by the following five methods: (1) no further correction (used to assess the 'worst case' scenario); (2) average artifact subtraction as proposed by Allen (Allen et al., 2000); (3) optimal basis set (OBS), as proposed by Niazy (Niazy et al., 2005); (4) combination of OBS and independent component analysis (OBS-ICA), as proposed by Debener, (Debener et al., 2007); and (5) CWL. See Table 1 for the parameters used in each artifact correction method. When correcting using OBS-ICA, we used the fastica implementation to transform the EEG into component activations and its weighting matrix. We removed (only) one ICA component that most resembled the BCG artifact. Finally, EEG data was transformed back again. These operations were performed using the meegpipe toolbox.

Assessment of EEG data artifact subtraction and He pump status

The measurement and artifact correction protocol produces 11 EEG data sets for each subject. The set representing the EEG traces obtained outside the magnet room is used as reference, or gold standard. The other 10 data sets result from the five different artifact subtraction methods, applied to both the He pump off and on assessments. All 10 sets are compared both with the reference set obtained outside the magnet, and with each other. The quality of the different artifact-corrected sets was firstly assessed by basic spectral signal-to-noise (SNR) and, secondly, by the presence of alpha power differences between eyes open and eyes closed conditions. As a finer-grained third assessment we quantified for each of the ten sets the regressor strength of naturally occurring fluctuations of EEG alpha power predicting fMRI blood-oxygenation level dependent (BOLD) activity.

Evaluation metrics

Signal-to-noise — relative distance of power spectra

As a quality measure for the artifact correction during the entire recording, we compare the power spectrum of the 10 MR- and BCG corrected EEG datasets obtained inside the scanner with the power spectrum of the EEG dataset obtained outside the magnet room, using the *relative distance*: the distance between a spectrum and the gold standard outside spectrum, expressed as a percentage of the size of the outside spectrum. This is in essence a normalized version of the Euclidean distance metric (Aggarwal et al., 2001) that is related to the RMSE divided by the L2 norm as follows:

$$\text{Distance} = \frac{\sqrt{\sum_i \left(S_{\text{IN}}(f_i) - S_{\text{OUT}}(f_i)\right)^2}}{\sqrt{\sum_i \left(S_{\text{OUT}}(f_i)\right)^2}} * 100\% \quad (4)$$

Where $S_{\text{IN}}(f_i)$ and $S_{\text{OUT}}(f_i)$ are the artifact-corrected spectra inside and outside the scanner respectively defined at frequency f_i. This relative distance measure approaches zero when spectra have comparable frequency characteristics and expresses differences as a percentage of the 'outside' EEG power.

Alpha Power — Jaccard overlap in alpha power difference

In most subjects, EEG alpha waves appear when the eyes are closed; these are called "Berger waves" (Kirschfeld, 2005). This increase in EEG alpha power in the 'eyes closed' condition, relative to the 'eyes open' condition is used as one of the outcome measures of the artifact correction and will henceforth be called the EO/EC effect. Since the EO/EC effect is different for each subject in terms of both the frequency band as well as the contribution per channel (i.e. topological distribution), we aimed to obtain a subject-specific measure of these properties: for the frequency band we determined an upper and lower frequency threshold (i.e., those frequencies in which the EO/EC effect is most pronounced), for the topological distribution we determined a channel selection (i.e., in which channels the EO/EC effect is most pronounced), and a vector specifying for each selected channel the contribution to the total EO/EC power increase.

To determine the upper and lower frequency thresholds, EEG data of the outside measurement was divided into two traces: one with eyes open and one with eyes closed. The power spectrum between 0 and 25 Hz was calculated for both traces. Examining the averaged power in the posterior channels (Pz, PO3, POz, PO4, Oz, Iz) allowed the identification of a frequency band related to the EO/EC effect. The lower and upper boundary frequency values of this band were defined at the frequency where the power increases at least 10% of the maximum increase across all posterior channels. Lower and upper frequency limits could not be lower than 7.5 Hz and 12.5 Hz, respectively. In five out of eight subjects, the EO/EC effect was pronounced, and boundaries could clearly be delineated; in the other three subjects, the EO/EC effect was very limited, but it was still possible to define a lower and upper frequency value. Once lower and upper frequency values were determined, the total EO/EC power increase (within the EO/EC frequency band) was calculated for every channel.

To select channels in each subject exhibiting the EO/EC effect, a (middle) threshold value was calculated as half of the sum of the minimum and maximum EO/EC power increases across channels. All channels for which the EO/EC power increase was greater than this middle threshold value were included in the selection. We also calculated a weighting vector specifying the relative contribution of each selected channel to the total EO/EC power increase found in the selected channels.

Table 1
Parameters used for the different artifact correction steps.

Artifact correction	Correction parameters	Software used
MRI correction (Allen et al., 2000; Moosmann et al., 2009)	Buffer: 25 MRI artifacts, buffer reset at 0.3 mm movement between EPI scans	Matlab, Moosman Plugin
CWL (Windowed Regression, see Methods)	Window length 4 s, time parameter 21 ms, taper factor 1, Hann window	Matlab, CWL Regression Tool
OBS-ICA (Debener et al., 2007)	Same as OBS, but with additional step in which 1 extra component is removed using ICA	Matlab, Meegpipe (Gomez) (http://meegpipe.github.io/meegpipe)
OBS (Niazy et al., 2005)	25 BCG artifacts, 3 additional Principal Components	Matlab, EEGLAB
AAS (Allen et al., 1998)	25 BCG artifacts	Brain Vision Analyzer
No BCG Correction	No further filtering operations after MRI correction. ECG markers are placed with Brain Vision Analyzer according to Christov, 2004 (Christov, 2004) and used for all other artifact corrections.	

Since the EO/EC effect is different in each subject, the number and location of selected channels was vastly different between subjects (see the white dots in Fig. 6A and the supplementary material). However, a common pattern emerged where the EO/EC effect was mostly comprised of posterior channels. For each subject, the channel selection and weighting vector was used to construct two weighted and averaged spectra (one for eyes open and one for eyes closed) which were used in further analyses.

For each artifact-corrected dataset in the MRI scanner, the same frequency boundaries, channel selections and channel weights were used to construct two weighted and averaged EO and EC spectra for further analysis (Fig. 5).

To evaluate the similarity of eyes-closed alpha power increase derived from artifact-corrected EEG recorded inside the scanner, as compared to the reference eyes-closed alpha power increase recorded outside the magnet room, two alpha power surface areas are considered. Surface in this case is defined as the area between the EO spectrum, the EC spectrum and the two alpha boundaries, and it represents the EO/EC effect in a spectral form (Fig. 5, upper part). This allows calculating the *overlap* of alpha power surface areas between the inside and outside situations using the Jaccard overlap index. This is mathematically defined as the intersection area between the inside and outside spectral surface areas divided by their union. Suppose that $R_{closed}(f_i)$ and $R_{open}(f_i)$ are the reference (outside) spectral values for any frequency f_i and that $Y_{closed}(f_i)$ and $Y_{open}(f_i)$ are the artifact-corrected spectral values at the same frequency f_i, then the Jaccard overlap index is given by the following formula:

$$J_{overlap} = \frac{\sum_{f_L \le f_i \le f_U} \left[Y_{closed}(f_i), Y_{open}(f_i)\right] \cap \left[R_{closed}(f_i), R_{open}(f_i)\right]}{\sum_{f_L \le f_i \le f_U} \left[Y_{closed}(f_i), Y_{open}(f_i)\right] \cup \left[R_{closed}(f_i), R_{open}(f_i)\right]} \quad (5)$$

where f_L is the lower alpha boundary and f_U is the upper alpha boundary value for f_i. In other words, the only situation where the Jaccard equals 1 is the situation where the eyes open spectra of both conditions ($Y_{open}(f_i)$ and $R_{open}(f_i)$) are exactly identical, and also the eyes closed spectra of both situations ($Y_{closed}(f_i)$ and $R_{closed}(f_i)$) are identical. Any other situation (even when spectra for outside and inside are of similar shape but don't overlap due to being at different spectral amplitudes) will reduce the overlap index, towards zero in case of no overlap. Therefore the Jaccard overlap index used in this work strictly tests for exact comparability between artifact-corrected spectra during scanning and outside spectra, and for detecting the EO/EC effect.

Alpha Power — relative distance of topological distributions

The second metric with which the EO/EC effect is compared uses the power increase within the subject-specific frequency band to the EO/EC effect, determined for each channel. This topographical distribution of alpha power can be written as a vector, and therefore be used as an input for the relative distance metric:

$$\text{Topological Distance} = \frac{\sqrt{\sum_i \left(D_{\text{IN},i} - D_{\text{OUT},i}\right)^2}}{\sqrt{\sum_i \left(D_{\text{OUT},i}\right)^2}} \quad (6)$$

Where $D_{IN,i}$ and $D_{OUT,i}$ are the alpha power increases for the artifact-corrected data inside and outside the scanner, at EEG electrode *i*. For each artifact-corrected data set, the topological distribution was compared with the 'gold standard' outside topological distribution (Fig. 6B). A lower relative distance means that the topological distribution is more similar to the outside distribution.

The above two metrics — the Jaccard overlap in alpha power difference, as well as the relative distance of topological distributions, allow a quantitative assessment of spectral and topological similarity of the EO/EC effect obtained from artifact-corrected EEG sets obtained in the scanner, as compared to artifact-free data obtained outside of the scanner.

EEG/fMRI BOLD analysis on alpha power fluctuations

The metrics described in the above sections (relative distance of the power spectra, Jaccard overlap in alpha power difference and relative distance of topological distributions) are all similarity assessments of EEG that is *averaged* over time. In order to also compare the artifact correction algorithms and He pump status (on or off) with respect to the extent to which the resulting traces are of value to track EEG *dynamics*, we evaluated the predictive value of derived alpha power fluctuations as a regressor for concurrent BOLD signal variation in time, using a General Linear Model (GLM) approach (Friston et al., 1995; Goldman et al., 2002).

First, a time-frequency representation (TFR) was calculated for each channel within windows with a length of TR to couple the temporal resolution to the MRI data, using the FieldTrip toolbox (Oostenveld et al., 2011). TFRs were then averaged using the same subject-specific channel selection and channel weights as in the previous section, to obtain a single time-frequency representation for each artifact-corrected EEG trace. The individual EO/EC frequency band boundaries were then used to obtain a single vector for alpha power fluctuations (see Fig. 7 in the results section for an example). This vector was subsequently Z-transformed and convolved with the hemodynamic response function (HRF) to obtain an alpha power regressor, which was entered into a GLM as effect of interest, in addition to the common 'nuisance' regressors of head motion realignment parameters.

FMRI data were pre-processed and analyzed using SPM8. Both He pump-off and He pump-on datasets were initially realigned to the first volume and slice-time corrected with the first slice used as a reference. Data were then co-registered to the standard MNI template and spatially smoothed with a 7-mm full width at half maximum (FWHM) kernel.

Multiple-participant, fixed-effects analyses were performed to assess the impact of different EEG artifact correction algorithms as well as He pump on/off in terms of their correlation with the underlying BOLD signal. For these fixed effects analyses, voxels were considered significant at a family-wise error (FWE) corrected threshold of $p < 0.05$. The small size of the current sample precluded meaningful random-effects analysis. However, inter-subject variability is not an issue for our comparisons, since these analyses only vary with respect to the BCG artifact correction applied to data — all underlying BOLD and (uncorrected) EEG data are identical.

Activation in the visual cortex was assessed by placing 8-mm spheres in the visual cortex (left and right) on the activation maxima as found in the group activation of the block GLM, and averaging the T-score of the negative alpha power contrast. Higher T-scores indicate better artifact correction performance because the artifact-corrected EEG explains more T_2^* variation.

Results

In the following three sections, figures are presented in pairs — first a figure for single subject to illustrate how a key parameter is obtained, followed by another figure illustrating how this parameter varies across all subjects for He pump on/off states and across all different artifact corrections. The supplementary data published in 'Data in Brief' (van der Meer et al., Submitted for publication) contains all other single-subject figures, which are in sub-sections with the same number and title as the sections here.

R peak detection and EO/EC effect

Accurate detection of R-peaks, essential for BCG correction, was suboptimal in the following cases (see Supplementary material section S2.4). In Subject 2, Helium pump off, detection of R peaks was possible, but motion in the EEG could interfere with accurate BCG correction

using AAS/OBS/OBS-ICA. In subject 4, both for Helium pump off and on, the ECG channel was saturated — but this subject displayed almost no EO/EC effect so is not included in further analysis. In subject 6, for Helium pump on, the ECG channel was saturated, making detection of R-peaks difficult. However, the EO/EC effect was almost as pronounced as in the He pump off condition. In subject 8, for both Helium pump conditions, detection of R-peaks was difficult. Summarizing, the (ideal) cases where both R-peaks could accurately be detected and where there was also significant EO/EC effect, were subjects 3 and 7. The other subjects which displayed a significant EO/EC effect — subjects 2 (during He pump off), 6 and 8 (both conditions), warrant more careful consideration.

Signal-to-noise — relative distance of power spectra

Upon visual examination (see Fig. 2 for an example EEG trace of one subject), the EEG trace recorded outside the magnet room always has the highest signal to noise (SNR) ratio: Alpha power can be seen throughout the trace (the condition is 'eyes closed') without any obvious artifacts. Fig. 2 shows that the EEG trace that is only corrected for MRI gradients contains the most noise. Fig. 2 also shows that the four BCG artifact-corrected EEG traces (one trace for each artifact correction method) look less noisy than the uncorrected trace, but still noisier than the trace recorded outside the magnet. The uncorrected-, AAS, OBS-, and OBS-ICA-corrected EEG traces show lower-frequency fluctuations that are absent in the CWL corrected trace and the outside trace. In the uncorrected-, the AAS-, OBS-, and OBS-ICA-corrected traces, the He pump artifact can be seen as diffuse bursts that contain power in higher frequencies. This effect differs greatly between subjects and between He pump systems. These bursts are equally present in the traces without BCG artifact correction and the AAS-, OBS-, and OBS-ICA-corrected traces. The He pump effects are removed in the CWL artifact-corrected EEG trace.

The above mentioned differences are clearly revealed in the EEG power spectra. Fig. 3 shows spectra of one subject. Examination of these averaged power spectra show that during MRI scanning, the artifact-corrected MRI spectra still contain peaks at the base frequency and all harmonics of the slice frequency (n slices/TR): 15.38 Hz for Verio and 15 Hz for Trio. However, this power is reduced compared to a situation where the SyncBox is deactivated or missing.

For the subject in Fig. 3 (i.e., subject 7), the power at the 2nd and at the higher harmonics of the MRI artifact is higher than expected with a perfect SyncBox function; for the other subjects (see 'Data in Brief' paper by van der Meer, et al.), this was not the case. Since the power at the base frequency and the 1st harmonic was suppressed sufficiently and we could accurately calculate alpha power differences, we chose to include this subject in the analyses.

The Helium pump introduces extra artifacts in the EEG trace, expressed as a collection of narrow peaks of varying height across a wide spectral range, starting at a frequency of about 40 Hz. The size of the He pump artifact differs between subjects (see Supplementary data), but the shape is scanner-specific.

The magnitude of the contribution of these artifacts to the spectrum differs greatly between subjects. Furthermore, the shape of the artifact spectrum is different for the Trio and the Verio system. Whereas the Trio magnet produces a He pump artifact with fewer peaks that are spaced more evenly across the spectrum, the Verio magnet generates He pump artifacts with many more peaks that are closer together. In all cases, switching on the He pump adds more noise to the data (Fig. 4A), increasing the relative distance with the 'outside' EEG power spectrum, especially due to contributions at higher frequencies (>25–30 Hz). The CWL-corrected traces show a reduced impact on trace quality due to the He pump, as indicated by a reduced distance with the outside EEG power spectrum (Fig. 4B) compared to all other artifact corrections (Fig. 4C). Regardless of the artifact correction algorithm used (AAS, OBS or OBS-ICA), the distance with the power

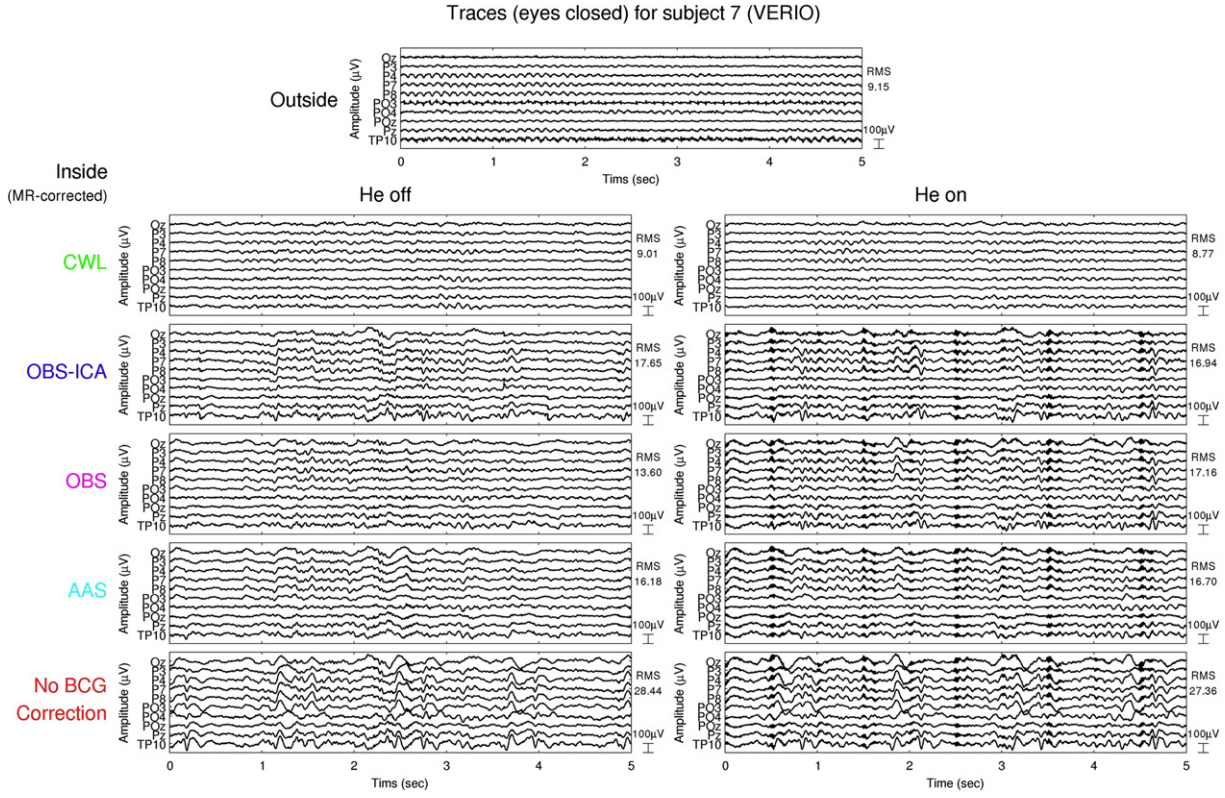

Fig. 2. Sample traces (5 s, 10 channels) for subject 7, as recorded outside the MRI room, as well as inside the MRI (but corrected for MRI) for different BCG artifact correction methods both for Helium pump off and on conditions. Notice that for a) AAS, OBS and OBS-ICA, more 'slow' wavelike activity is present. b) The He pump produces a bursting-like pattern.

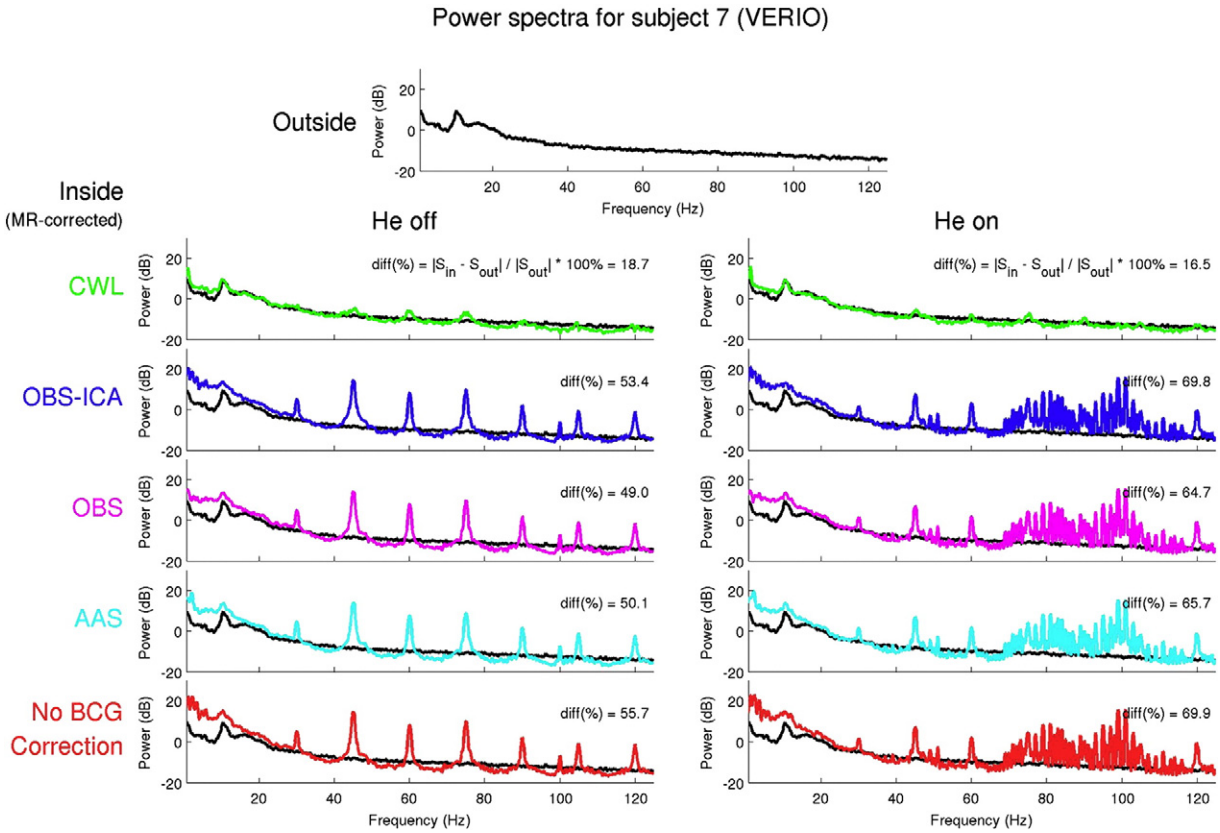

Fig. 3. Power spectra (averaged over EEG channels) for different BCG artifact correction algorithms, compared to the power spectrum of the EEG trace outside. Notice that: a) for AAS, OBS and OBS-ICA, residual MRI artifact peaks are present in the power spectrum; b) for the He pump on condition, more high-powered peaks appear at frequencies of 60–120 Hz, c) at low frequencies (0–25 Hz), the power is 5–10 dB higher than the outside spectrum. The relative distance between the power spectrum (colored) and the spectrum outside of the MRI scanner (black) is written as d_{abs}.

spectrum of the EEG signals obtained outside of the scanner remains high, and only for the CWL artifact correction, the distances decreased markedly.

Additionally, the spectra show that the BCG power is most pronounced in frequency ranges between 0 and 25 Hz. Applying any artifact correction reduces this power by about 10 dB, but does not completely remove it. Only the CWL-corrected trace produces a spectral power between 0 and 25 Hz that is comparable to the power that can be measured outside (see Fig. 3).

Alpha Power — Jaccard overlap and relative distance of topological distributions

In three out of eight subjects (subjects 1, 3, and 8), the EO/EC effect was not clear, even in the reference EEG traces obtained outside the magnet room; this level of inter-subject variability is in line with previous EEG/fMRI studies (Goncalves et al., 2006; Goldman et al., 2002). These three subjects are therefore omitted for the comparisons in this section — see supplementary material, section S2.2, figures S2.2.1, S2.2.4 and S2.2.5 for their spectra and topographical distributions. As expected, there were individual differences in the lower and higher alpha boundary frequency values, as well as in the area defined by the power increase during 'eyes closed' relative to 'eyes open' between these boundaries (Fig. 5, upper panel). Fig. 5 shows the power spectra of 'eyes closed' and 'eyes open' EEG for a single subject, as well as the boundaries of the frequency range where the EO/EC effect occurs. For every artifact correction method, the area defined by these boundaries was compared to the area found in the EEG obtained outside of the scanner. The overlap is largest for the CWL artifact corrected trace; an average 0.53 (range: 0.28–0.72) across subjects (Jaccard range is 0–1). For AAS, the overlap was 0.18 (range: 0–0.49), for OBS the overlap was 0.18 (range: 0.09–0.42) and for OBS-ICA it was 0.14 (range: 0–0.38). There was no consistent increase or decrease depending on the He pump state.

When looking at the topological distribution of the alpha power increase produced by eye closure, the EEG assessed outside of the scanner always has the clearest topology of increased values near the Oz/POz/Iz electrodes (see Fig. 6) and individual differences with respect to lateralization and size of the topological distribution.

Fig. 6 provides an overview of the relative distances between the reference topological distribution obtained from the EEG recorded outside of the scanner, and the topological distributions obtained from the different artifact-corrected EEGs. The He pump state did not consistently increase or decrease the goodness of fit of the EO/EC effect's spatial distribution. The CWL artifact correction produces a topological distribution that is always more similar to the outside measurement than any of the other correction methods (AAS, OBS or OBS-ICA). One notable measurement is subject 3, who was scanned in the Trio. During the He pump off condition, the topological distance was much higher than during the He pump on condition, and this difference seemed to increase with artifact correction. Surprisingly, the OBS-ICA corrected EEG displayed yielded a more dissimilar topological distribution than the AAS and OBS — corrected data.

EEG/fMRI BOLD analysis on alpha power fluctuations

In order to examine alpha power fluctuations over time, time-frequency representations (TFR) were made for all EEG traces: See Fig. 7 for such a representation made for subject 6 (VERIO). The CWL artifact-corrected TFRs were most similar to the TFRs of the EEG data recorded outside of the scanner. The BCG-uncorrected trace had the

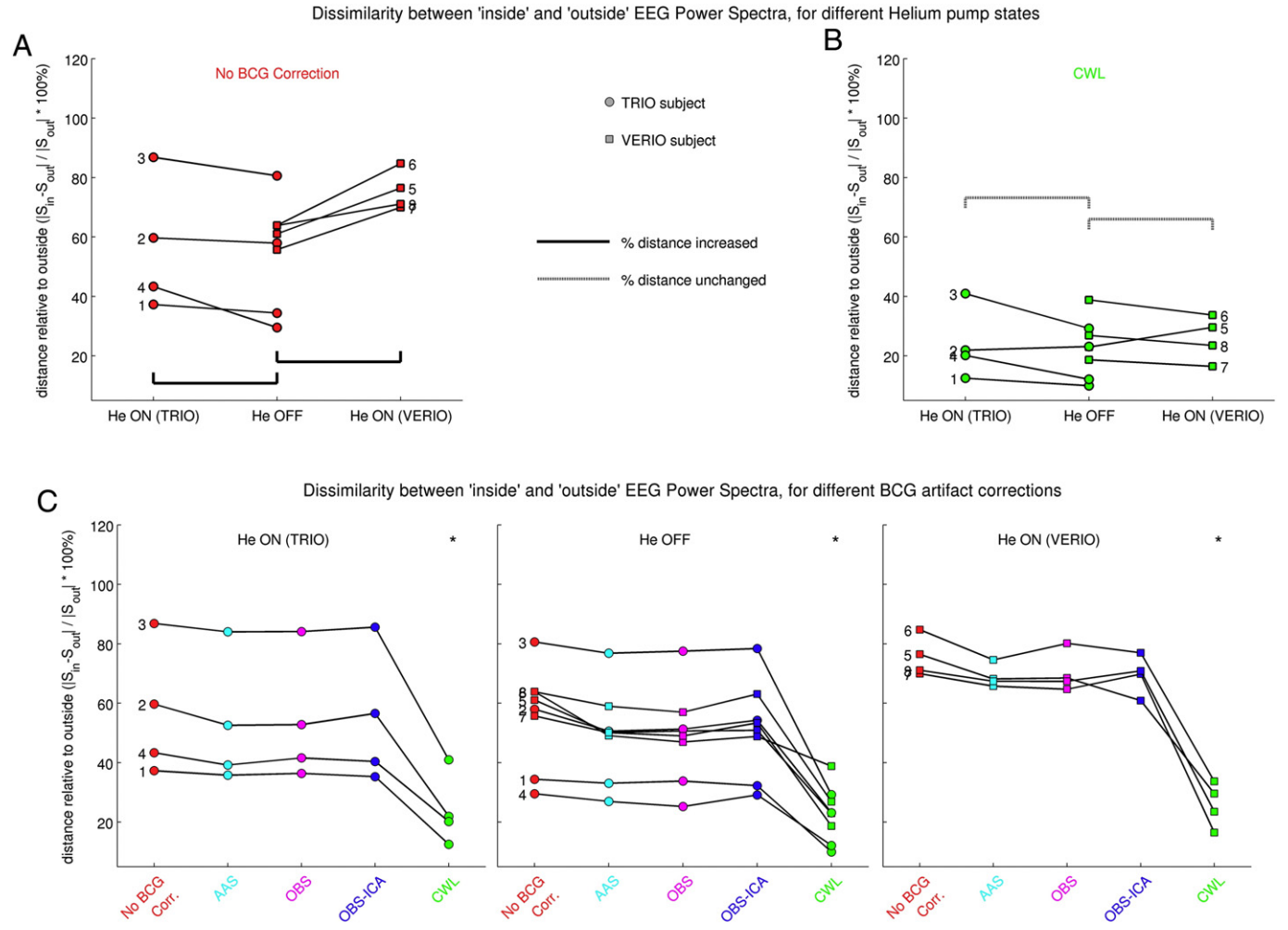

Fig. 4. (A): When the Helium pump system is switched on, the power spectrum becomes more dissimilar to the spectrum outside if no BCG artifact correction is performed — this is reflected in an increase of the relative distance between inside and outside power spectra (B): These distances do not change significantly, regardless of artifact correction (AAS, OBS or OBS-ICA). Only for the CWL artifact correction the distance is reduced markedly. (C): For the CWL corrected traces, whether the Helium pump is on or not does not increases the dissimilarity to the outside power spectrum.

most variability, and even hardly reflected the eyes open — eyes closed block design. Correction using AAS, OBS and OBS-ICA resulted in TFRs more similar to the TFRs of the EEG data recorded outside of the scanner, but still showed significantly more variability. An important observation is that time points with elevated power across a large frequency range (spikes) occur in the uncorrected, AAS, OBS, and OBS-ICA corrected traces. These were present at different scans throughout the measurement: in subject 1 at scan 42 (He off), subject 2 at scan 45 and 90 (He off), subject 4 at scan 55 (He off) and scan 82 (He on), subject 5 at scan 43 (He off), and finally subject 6 at scan 95 (He off, and shown in Fig. 7). These phasic spectral power increases were not present in the CWL-corrected trace. These periods coincide with periods in which the R-peak detection was not optimal — so they played no role in the assessment of the relative distance of power spectra, Jaccard overlap or the relative distance of topological EO/EC distribution. Furthermore, the CWL corrected spectrograms consistently show an alpha power signal that is cleaner and that is comparable to those found outside of the magnet, especially during eyes closed condition where alpha should be low and stationary. The Helium pump state does not affect alpha power fluctuations.

Fixed-effect group analysis of the BOLD correlates of (HRF-convolved) alpha power fluctuations show different distributions of BOLD activation, depending on the artifact correction used; see Fig. 8. Regardless of the artifact correction used, the visual cortex is activated in all cases. For the uncorrected EEG traces, significant BOLD effects can be seen in regions that should not be activated (e.g. vascular regions). For the EEG traces corrected with AAS, OBS and OBS-ICA, alpha power was correlated with BOLD activity in a spatially more distributed network across visual, motor and (frontal) cognitive brain areas. Bold activity correlated with alpha power fluctuation in the CWL-corrected EEG showing a much more spatially focused pattern in the visual cortex and parietal association cortices. Importantly, the BOLD correlation was also stronger (see Table 2): average T-scores from 8-mm spheres in the bilateral visual cortices showed that the CWL corrected traces had the highest T-scores compared to the AAS, OBS, and OBS-ICA corrected data. There was no effect in BOLD activation average T-score depending on the Helium pump state.

Discussion

Here, we introduced a carbon-wire signal-based artifact correction algorithm for simultaneous EEG-fMRI and compare its performance with three other state-of-the-art methods, focusing on how all correction algorithms function when the He pump was switched on or off. To this end, we firstly compared the artifact-corrected signal itself, in a range between 0 and 125 Hz, with the 'gold standard' reference of EEG recorded outside the magnet room. Second, we investigated helium pump state and artifact correction method used in terms of the EO/EC effect. Finally, we investigated artifact correction method used in terms

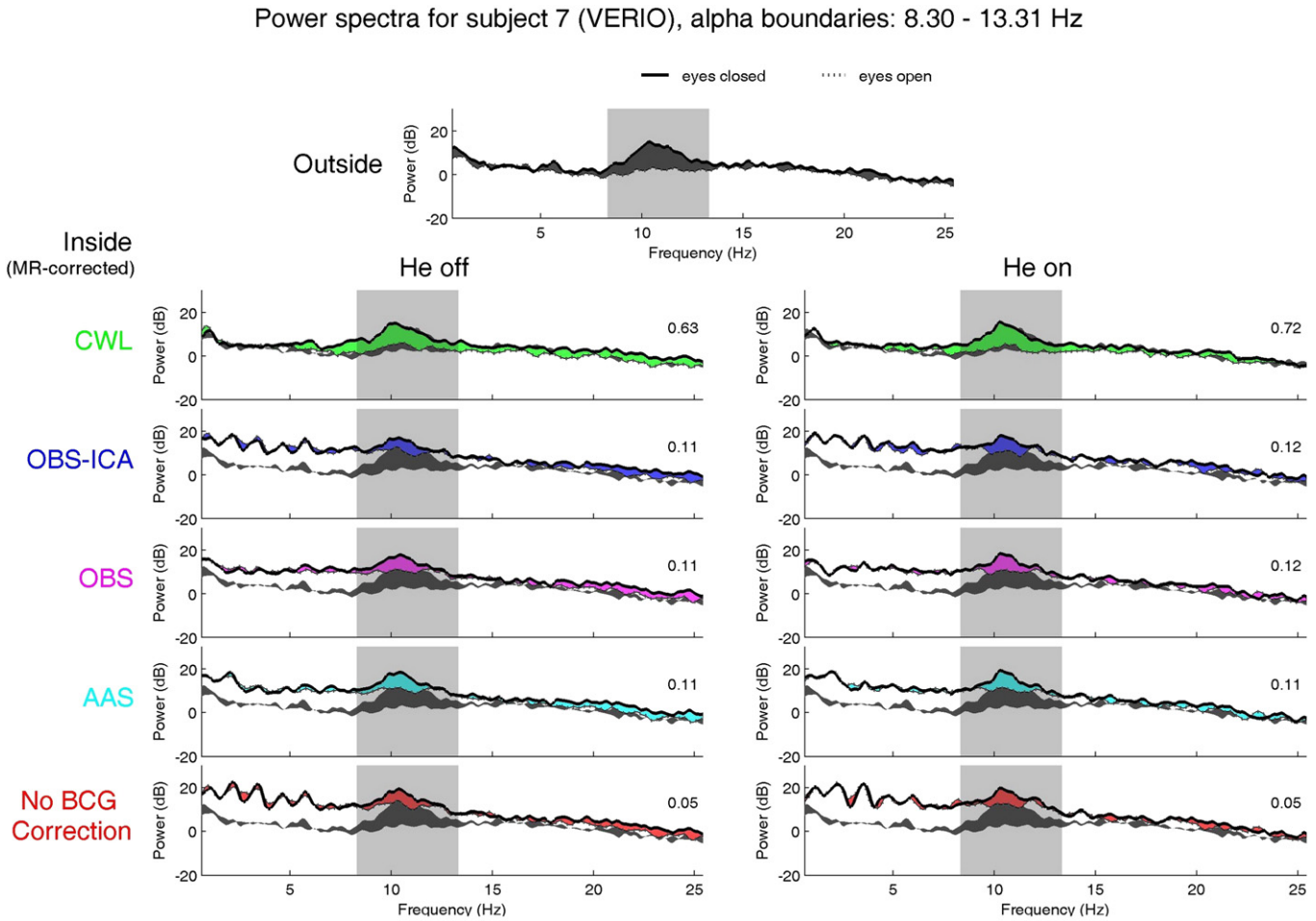

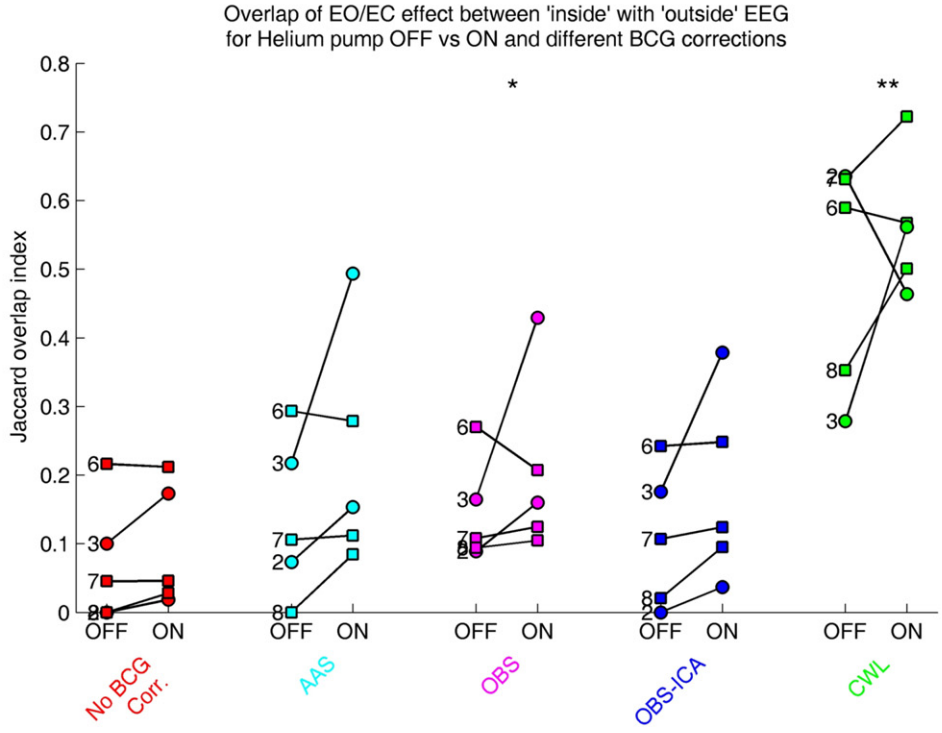

Fig. 5. (Top). The alpha power difference between the 'eyes closed' and 'eyes open' (EO/EC effect), for outside the MRI (plotted as the black surface in all graphs), and how this alpha power difference can be detected from the artifact-corrected EEG data inside (colored surfaces). The EO/EC frequency boundaries are depicted with the gray rectangular area. The Jaccard overlap index is shown in each graph. The power in the 0 to 10 Hz frequency range, relative to the outside spectrum, is markedly higher for AAS, OBS and OBS-ICA. The CWL correction produces power levels much more similar to the outside measurement at these lower frequencies. (Bottom): Jaccard overlap indices for all subjects in which the EO/EC effect could reliably be detected in the outside power spectra, for all artifact corrections and Helium pump states. The overlap for the AAS, OBS-ICA methods is relatively low; OBS seems to yield slightly increased overlap (*). The overlap increases markedly for the CWL artifact correction (**). The helium pump state does not affect the overlap.

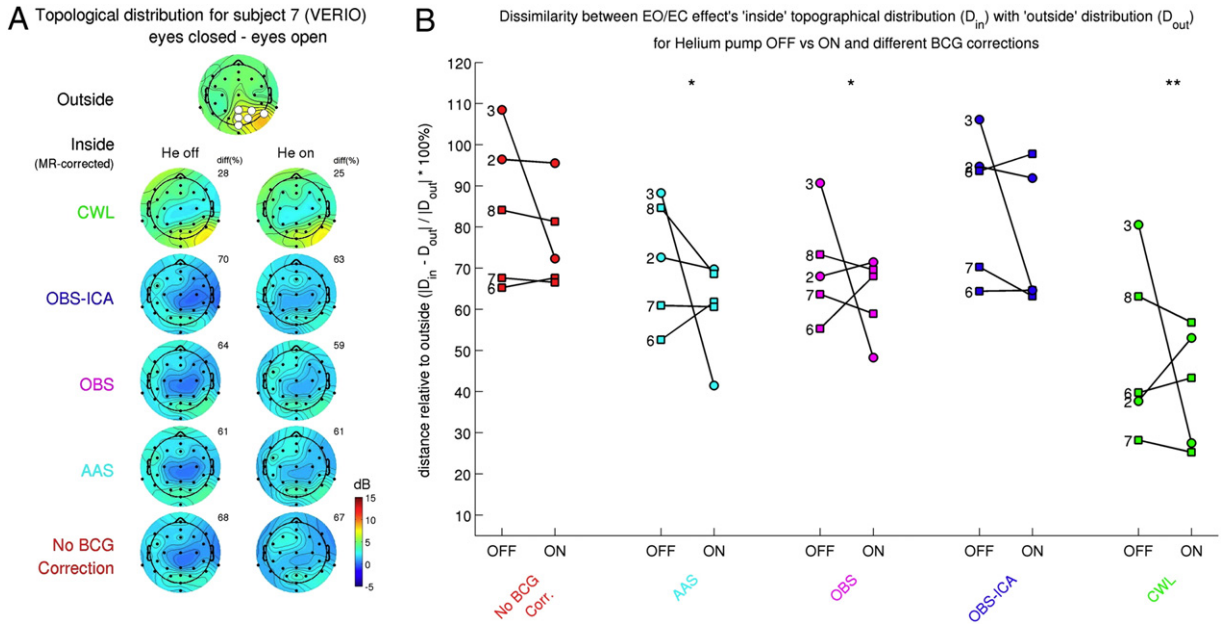

Fig. 6. (Top): Topological alpha power *difference* distributions (for alpha power boundaries; see also Fig. 5). The white dots indicate the channels which were used to create the averaged eyes open-eyes closed spectra of Fig. 5. (Bottom): relative distances between the topographical distribution with the outside topological distribution, for the 5 subjects in which the EO/EC effect could be detected outside of the scanner. (*) While the AAS and OBS (but not the OBS-ICA) corrections already improve the topological distribution, the improvement is the greatest with the CWL method (**), which yielded the lowest distance. The helium pump state does not affect the topological distribution.

of BOLD correlates of alpha power fluctuations, extracted from of the different artifact-corrected EEG data.

Signal-to-noise

When correcting only for MRI gradient artifacts, the time traces and spectra clearly show immense residual artifacts. Performing the AAS correction yields a marked improvement with respect to removing the low(er) frequency BCG artifacts, but these are not completely removed, as can be seen from the slow waves in the EEG traces, and power at lower frequencies (0–25 Hz) in the EEG spectra. Performing AAS removes the bulk of the BCG artifact, while the OBS and OBS-ICA corrections yielded only small incremental improvements. However, all three of the AAS, OBS, and OBS-ICA corrections do not successfully deal with artifact components at higher frequencies (consisting of high frequency components of the BCG and the MRI and He pump artifacts). This essentially forces the experimenter either to use more advanced analysis methods to remove these artifacts as well, or to choose to only focus on low-frequency EEG components for any experiment. The proposed CWL correction method is a considerable improvement as compared to AAS, OBS, or OBS-ICA. This conclusion is supported by the relative distance results shown in Fig. 4. Power spectra of EEG during scanning are considerably more similar to the power spectra of EEG recorded outside of the scanner, even when the Helium pump is switched on.

Alpha Power — spectra and topographical distribution (EO/EC effect)

A higher SNR, as derived from the relative distance relative to the 'gold standard' reference power spectrum of EEG, does not necessarily mean that physiologically meaningful fluctuations in the EEG are maintained. In the worst case, they might be discarded along with the BCG artifacts as an unwanted side-effect of the artifact correction procedure. It is, therefore, also necessary to investigate whether the correction procedure leaves the physiologically meaningful fluctuations in EEG intact. To do so, we chose to analyze the EO/EC effect (Kirschfeld, 2005) due to its robustness and insensitivity to experimental conditions. In our results, for BCG-uncorrected traces, the BCG artifact in some cases is so large that alpha power differences between 'eyes closed' and 'eyes open' cannot be noticed at all (see supplementary data, section S2.2). In other cases, the EO/EC effect can still be seen, in spite of these artifacts (see Figs. 5 and 6). Artifact correction using AAS, OBS, or OBS-ICA improves the signal, but to a lesser degree than the proposed CWL method, which yields a marked improvement on the ability to detect alpha power differences during eyes open and eyes closed.

Our finding that the He pump state does not systematically change the Jaccard overlap for any artifact correction method used may signify that, at least for frequency ranges between 8 and 13 Hz, the He pump state may be less relevant. The main power of the He pump artifacts, at least for the two different He pump systems in the current investigation, lies in frequency range above that of the alpha power (~25–50 for Trio, and ~30–100 for Verio). For the scanners we used, it seems possible to run paradigms that solely focus on alpha power, without the need to shut down the He pump. Whether or not this also holds true for other scanners and He pump systems remains to be evaluated. Preliminary testing of a phantom in a MAGNETOM Skyra scanner (Siemens Healthcare) showed a significant contribution of its He pump also at lower frequency ranges, with elevated power between 7 and 50 Hz, while, in contrast to the Trio and VERIO scanners, contributed less to frequencies above 60 Hz (not shown).

It should be noted that differences in the Jaccard index (spectral overlap of the EO/EC effect with the outside situation) between the helium pump on and helium pump off EEG data could have a physiologic origin. These two sessions may differ with respect to fatigue and comfort. The increase in this difference between helium pump states after the CWL correction, relative to the other corrections, may therefore indicate that the CWL correction method allows for a more sensitive detection of intrinsic physiological variation.

The results of the topological distributions of the EO/EC effects alpha power differences mirror the findings of the overlap in the frequency dimension. The CWL-corrected EEG data shows the most robust spatial distribution of the EO/EC effect. In fact, it was difficult to define robust topological distributions for all the other artifact correction methods, likely due to residual BCG artifacts.

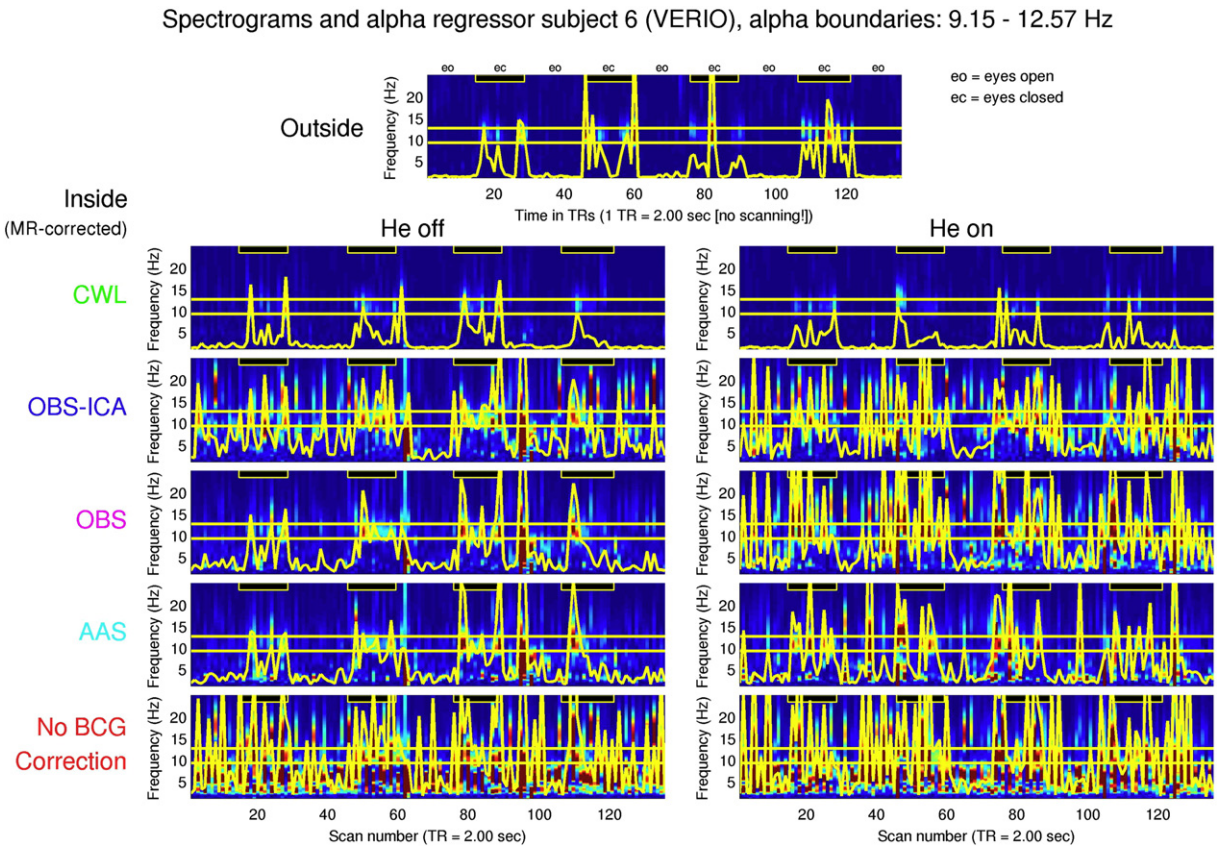

Fig. 7. Time-frequency decomposition (averaged over channels (see the white dotted channels from Fig. 6)) of the EEG signal, for one subject, all artifact correction methods and Helium pump states. Notice that the CWL loops have less sudden 'surges' in spectral power, as is seen with the AAS, OBS and OBS-ICA algorithms. The yellow vertical lines depict the alpha power 'EO/EC effect' boundaries. The yellow fluctuating line is the sum of the alpha power within these boundaries.

EEG/fMRI BOLD analysis on alpha power fluctuations

Artifact correction methods for simultaneous EEG/fMRI acquisitions need to be able to disambiguate between scanner induced artifacts and true EEG signal and remove the former, while leaving the latter intact. To determine if the variability in alpha power that remains after the artifact correction is likely to be physiologically meaningful, the aforementioned correlational analysis between EEG and BOLD-fMRI was performed. If an artifact correction procedure removes too much of real physiological signal, the extracted EEG feature would show lower correlations with the BOLD signal and produce lower t-scores in a standard GLM analysis approach. Therefore, EEG/BOLD-fMRI correlations can be used as an additional test for the validity of the artifact correction procedure.

The EEG/fMRI results (Fig. 8) show that alpha power fluctuations in the uncorrected traces are correlated to BOLD fluctuations in the expected region of the visual cortex. However, the t-values from the mask in the visual cortex are considerably lower than after applying any BCG artifact correction to the EEG. Furthermore, there are brain activations in unspecific areas, especially in the ventricles, possibly resulting from motion effects. The use of artifact correction with AAS, OBS and OBS-ICA enhances the correlation between the fluctuations in alpha power and visual cortex BOLD activation. In addition to the visual cortex, brain activation in a widely distributed network across the entire brain is suggested, in accordance with previous studies on the correlation between fluctuations in EEG alpha power and the fMRI BOLD signal (de Munck et al., 2009; Mantini et al., 2007). However, one study questioned the validity of BOLD activation in these non-visual cortical regions and suggested that it could be the result of motion artifacts (Jansen et al., 2012). The study showed suggestive motion-perception related BOLD activations in motor cortex, anterior cingulate cortex and insula, during a completely non-motion fMRI task. This likely resulted from motion-related artifactual signal leaking into the correlation between EEG and fMRI fluctuations (Jansen et al., 2012). Regarding such an investigation of motion, any dataset with hardware motion sensors would allow for this. Motion sensors (such as the CWL's) yield much more sensitive and specific information about motion than motion parameters obtained from functional MRI data. Motion could be detected and included into a GLM analysis as events to separate motion effects from the experimental design itself.

As compared to any other correction method suggested so far, the CWL artifact correction resulted in substantially higher t-values in a more restricted spatial distribution around the visual cortical area. It is therefore likely that the CWL artifact correction also reduces BOLD activation that is associated with subject motion, as it can account for sudden motion artifacts in the EEG.

On ICA approaches for EEG/fMRI artifact corrections

A critical note can be conveyed with respect to the use of ICA for the removal of the BCG artifacts. ICA in its currently used form implicitly assumes an identical temporal delay between one source and *all* the sensors. While this is true for electrical signals originating within the brain, it is not necessarily the case for all motion artifacts, including BCG. These artifacts may appear with different time delays across the different EEG sensors. Calhoun (Calhoun et al., 2003) proposed an ICA algorithm that can properly account for temporal delays in artifacts originating from the BCG or He pump. In our own investigations of the ICA decomposition of the He pump artifact, we routinely see up to three components that correlate with the He pump signal at different delays. The use of ICA for the removal of the BCG artifact with its variable range of timings is still a topic of ongoing research (Maggioni et al., 2014). Furthermore,

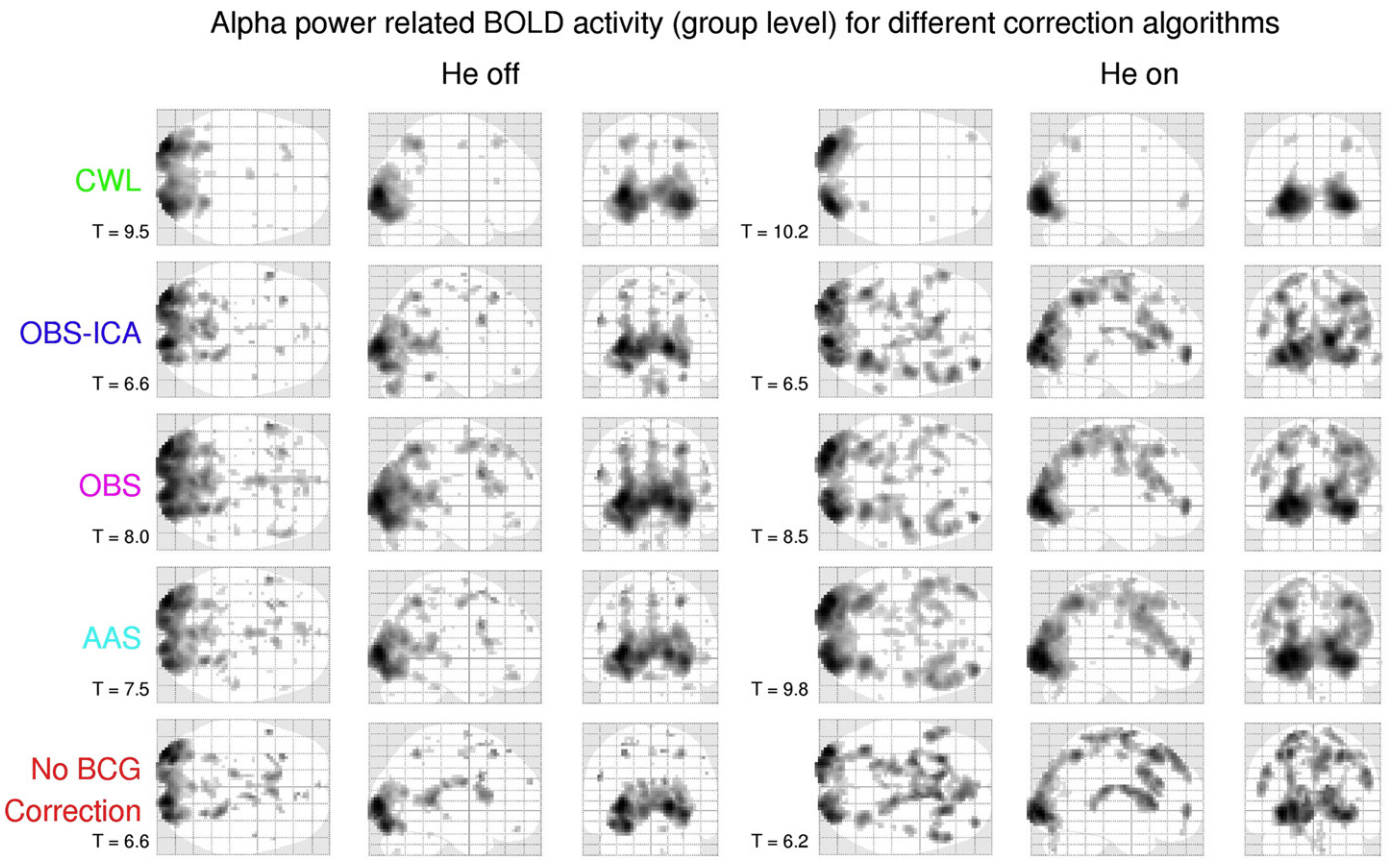

Fig. 8. Glass brain activation maps (Fixed-level group analyses of all 8 subjects, p = 0.05 FWE corrected) of BOLD that is anti-correlated with alpha power, which is modeled by convolving the yellow line in Fig. 7 with the canonical Haemodynamic Response Function. The CWL corrected data produces glass brains in which the activation is more confined to the visual cortex, without the extra activations in motor and cingulate cortices as seen with the AAS, OBS and OBS-ICA algorithms. The T-value consists of the average T-score within a mask comprising of 8-mm spheres in bilateral visual cortices. The T-values are the highest for the CWL correction. This effect is not different for different Helium pump states.

when the number of EEG channels is low, the likelihood that ICA components that seem to be artifactual in nature also contain some EEG signal increases. The results in Fig. 6 indeed hint that this could be the case for our data, even after removal of a single component. OBS-ICA might therefore not be ideal for our particular dataset, since we have only 30 EEG channels. There are many other possible OBS-ICA implementations, each of them more optimized for different situations. A good overview has been published (Vanderperren, et al., 2010) that discusses in great detail performance issues between $7 \times 4 \times 8 = 224$ possible OBS-ICA implementations on a 64 channel EEG data set. We will opt to release our raw data in the 'data in brief' journal (van der Meer et al., Submitted for publication) format, to allow other groups to test performance with their own OBS-ICA implementation.

In addition to AAS, OBS, and OBS-ICA, several other BCG correction algorithms for EEG/fMRI artifact have been proposed. Two of them are likely to yield results that are comparable with those found in this paper, either because of realistic assumptions of the underlying physical phenomena (de Munck et al., 2013), or because of the inclusion of hardware-based reference signals, such as the 'quad cable' (Chowdhury et al., 2014) or 'BCG net' (Luo et al., 2014). In terms of ease of use, the CWL solution does not require custom-made EEG cap with quad cables, nor does it run the risk of significantly suppressing the MRI signal as could be the case with the BCG net.

Table 2
Average T-values of the correlation between EEG alpha power and BOLD signal of voxels within 8-mm masks of bilateral visual cortices.

Artifact correction	T-value (EEG alpha power — BOLD signal) within 8-mm spheres placed on bilateral visual cortices	
	He pump off	He pump on
CWL	9.5	10.2
OBS-ICA	6.6	6.5
OBS	8.0	8.5
AAS	7.5	9.8
No BCG correction	6.6	6.2

The simplicity of the CWL artifact correction algorithm makes it ideally suited for a real-time implementation. Current EEG/fMRI artifact correction methods require extensive and time consuming processing involving visual inspection of ECG traces, inspection of ICA results, and sufficient computing power. The only real-time artifact correction method to date which is readily available in real-time is the AAS algorithm implemented in the RecView software (Brain Products, Gilching, Germany). Our observations suggest that the CWL method would allow for real-time cleaning and result in EEG signals with a quality that is comparable to those obtained outside the scanner. This is especially important for neurofeedback research and applications. Real-time EEG feedback requires a high-quality EEG signal because the lack of time limits the postprocessing and artifact correction algorithms that are feasible. A real-time implementation of the CWL method promises high-quality EEG for neuro-feedback studies linking the EEG and fMRI realms (Becker et al., 2011; Chang et al., 2013; Zotev et al., 2014). Real-time application however remains to be evaluated.

Study limitations

Regarding the 0.3 mm threshold in our MR artifact correction: while we checked carefully that the 0.3 mm cut-off threshold for window rebuffering worked out well to obtain a constantly well-corrected EEG timecourse, one needs to acknowledge that such parameters may have to be seen as specific for our conditions of field strength, spatial

resolution and overall subject motion. While for a real-time hardware correction approach a window based MR-template estimate for MR artifact removal is essential, for an off-line correction approach other MR removal methods are be better suited. Future work may investigate in depth how cluster based approaches perform in comparison with the windowed template generation, if no realtime correction is intended. A thorough evaluation of the different MR artifact correction algorithms and how they compare to each other is currently missing in the literature, which instead focuses on assessment of different BCG correction algorithms on the final (cleaned) signal. We publish our raw data in the 'Data in Brief' format (van der Meer et al., Submitted for publication) in order to facilitate such comparisons by other research groups.

Sub-optimal detection of R-peak markers in the ECG trace possibly impact the results with regard to the comparison of different artifact methods using the Jaccard overlap of EO/EC effect's spectral power (Fig. 5), and using the topological relative distance (Fig. 6). For Subjects 2 (only for Helium pump OFF condition), 6 and 8 (both conditions), R-peak detection was challenging. Therefore, in these cases the CWL correction might have been unfairly advantaged over the other artifact corrections (AAS, OBS and OBS-ICA) — and these artifact corrections could potentially perform better than as reported in this paper. The same holds true for the EEG/fMRI BOLD assessment. In this case, we had to use all the EEG data — even parts which were omitted from the previous two comparisons. Accordingly, a more fair comparison would be possible if we had more data to allow omitting all the data where R-peak detection was difficult.

Regarding R-peak detection, it is a common occurrence that the ECG channel quality is compromised in EEG-fMRI, often to a point where detection is not possible in the case of 'poor' ECG traces (Niazy et al, 2005). This issue depends on MRI sequence parameters and orientation of the ECG lead in the magnetic field. However, even controlling for these issues does not always help, and quality could become compromised *during* a measurement. For the CWL correction, the considerable time and effort in detecting R-peaks from the ECG channel for the most optimal BCG artifact correction performance, and its consideration into assessment of EEG results, are a non-issue; accordingly, rejection of measurements due to compromised R-peak detection can be averted with CWL.

Conclusion

Obtaining high quality EEG signals in the MRI scanner remains difficult. The electrical signals of interest that originate in the brain are mixed with largely unpredictable artifactual signals due to MRI scanning (the gradient artifact) and semi-regular motion such as heart beats (the BCG artifacts), the He pump, and motion of the subject itself (coughing, slight alterations of the head position, jerky motions). Sophisticated artifact cleaning procedures are indispensible, and require close examination to ensure true brain signals of interest are not misclassified as artifacts and removed or spurious signal introduced. Or vice versa that these artifacts, some of them closely resembling true brain activity, remain in the EEG as residuals that are treated as true brain activity. The artifacts from MRI scanning and motion in the $\mathbf{B}_0$ field are so large, that it is almost unavoidable to accept some remaining residuals, making it difficult to distinguish between artifact and true brain activity. To address this issue, a practical way to evaluate the EEG cleaning procedure is to determine EEG usability for specific applications. Therefore, in the present study we evaluated the EO/EC effect and the covariation between fluctuations in EEG alpha power and the BOLD-fMRI signal.

The use of CWLs to capture BCG and He pump artifacts allows the researcher to obtain accurately cleaned EEG even in a situation where the He pump is still active. Additionally, the CWL artifact method outperformed conventional software-based AAS, OBS, and OBS-ICA methods in removing BCG artifacts. Furthermore, visual inspection of the CWL signals themselves is extraordinarily useful in manual data rejection procedures when assessing artifact-corrected EEG data (such as with the scoring of sleep EEG data in EEG/fMRI experiments) — the signals show whether or not a motion occurred throughout the entire recording.

CWL regression produces an artifact-corrected signal that is much more comparable to EEG recorded outside of the scanner. Using the CWL setup has several benefits: the regression requires neither the detection and visual inspection of R-peak markers, nor the visual inspection and selection of ICA components to remove. Both of these steps require time consuming manual intervention. In addition, the system allows increasing the EEG/fMRI throughput by enabling longer measurement sessions without the need to switch off the He pump, which is especially useful for longer sleep EEG/fMRI recordings. Furthermore, CWL's can be used with any scanner type or EEG system, as long as recording of bipolar channels is possible. These advantages will be pivotal in developing a real-time EEG correction method that will strongly facilitate stimulation time-locked to oscillations, as required for example for neuro-feedback.

Acknowledgments

We would like to thank and acknowledge Andrew Webb, for taking the time to visit Amsterdam and getting us started in the construction of the carbon-wire loops. In addition, we thank Anton Lord for critically proof-reading this manuscript. This work was supported by Netherlands Organization for Scientific Research (NWO) grants: VICI 453.07.001 to EJWVS, VIDI 016.095.359 to YDVDW. Furthermore, this work was supported by the German Research Foundation (DFG) grant SFB779 to MW.

Appendix A. Supplementary data

Supplementary data to this article can be found online at http://dx.doi.org/10.1016/j.neuroimage.2015.10.064.

References

Abbott, D.F., Masterton, R.A.J., Archer, J.S., Fleming, S.W., Warren, A.E.L., Jackson, G.D., 2015. Constructing carbon fiber motion-detection loops for simultaneous EEG-fMRI. Front. Neurol. 5 (10.3389).

Aggarwal, C.C., Hinneburg, A., Keim, D.A., 2001. On the Surprising Behavior of Distance Metrics in High Dimensional Space. Springer.

Allen, P.J., Polizzi, G., Krakow, K., Fish, D.R., Lemieux, L., 1998. Identification of EEG events in the MR scanner: the problem of pulse artifact and a method for its subtraction. NeuroImage 8, 229–239.

Allen, P.J., Josephs, O., Turner, R., 2000. A method for removing imaging artifact from continuous EEG recorded during functional MRI. NeuroImage 12, 230–239.

Becker, R., Reinacher, M., Freyer, F., Villringer, A., Ritter, P., 2011. How ongoing neuronal oscillations account for evoked fMRI variability. J. Neurosci. 31, 11016–11027.

Calhoun, V.D., Adali, T., Pekar, J.J., Pearlson, G.D., 2003. Latency (in)sensitive ICA. NeuroImage 20, 1661–1669.

Chang, C., Liu, Z., Chen, M.C., Liu, X., Duyn, J.H., 2013. EEG correlates of time-varying BOLD functional connectivity. NeuroImage 72, 227–236.

Chowdhury, M.E.H., Mullinger, K.J., Glover, P., Bowtell, R., 2014. Reference layer artefact subtraction (RLAS): a novel method of minimizing EEG artefacts during simultaneous fMRI. NeuroImage 84, 307–319.

De Munck, J.C., Goncalves, S.I., Mammoliti, R., Heethaar, R.M., da Silva, F.H.L., 2009. Interactions between different EEG frequency bands and their effect on alpha-fMRI correlations. NeuroImage 47, 69–76.

De Munck, J.C., van Houdt, P.J., Gonçalves, S.I., van Wegen, E., Ossenblok, P.P.W., 2013. Novel artefact removal algorithms for co-registered EEG/fMRI based on selective averaging and subtraction. NeuroImage 64, 407–415.

Debener, S., Strobel, A., Sorger, B., Peters, J., Kranczioch, C., Engel, A.K., Goebel, R., 2007. Improved quality of auditory event-related potentials recorded simultaneously with 3-T fMRI: removal of the ballistocardiogram artefact. NeuroImage 34, 587–597.

Debener, S., Mullinger, K.J., Niazy, R.K., Bowtell, R.W., 2008. Properties of the ballistocardiogram artefact as revealed by EEG recordings at 1.5, 3 and 7 T static magnetic field strength. Int. J. Psychophysiol. 67, 189–199.

Delorme, A., Makeig, S., 2004. EEGLAB: an open source toolbox for analysis of single-trial EEG dynamics including independent component analysis. J. Neurosci. Methods 134, 9–21.

Friston, K.J., Holmes, A.P., Poline, J.B., Grasby, P.J., Williams, S.C.R., Frackowiak, R.S.J., Turner, R., 1995. Analysis of FMRI time-series revisited. NeuroImage 2, 45–53.

Goldman, R.I., Stern, J.M., Engel, J., Cohen, M.S., 2002. Simultaneous EEG and fMRI of the alpha rhythm. NeuroReport 13, 2487–2492.

Goncalves, S.I., de Munck, J.C., Powels, P.J.W., Schoonhoven, R., Kuijer, J.P.A., Maurits, N.M., et al., 2006. Correlating the alpha rhythm to BOLD using simultaneous EEG/fMRI: inter-subject variability. NeuroImage 30, 203–213.

Grouiller, F., Vercueil, L., Krainik, A., Segebarth, C., Kahane, P., David, O., 2007. A comparative study of different artefact removal algorithms for EEG signals acquired during functional MRI. NeuroImage 38, 124–137.

Jansen, M., White, T.P., Mullinger, K.J., Liddle, E.B., Gowland, P.A., Francis, S.T., Bowtell, R., Liddle, P.F., 2012. Motion-related artefacts in EEG predict neuronally plausible patterns of activation in fMRI data. NeuroImage 59 (1), 261–270.

Kirschfeld, K., 2005. The physical basis of alpha waves in the electroencephalogram and the origin of the "Berger effect.". Biol. Cybern. 92, 177–185.

Liu, Z., de Zwart, J.A., van Gelderen, P., Kuo, L., Duyn, J.H., 2012. Statistical feature extraction for artifact removal from concurrent fMRI-EEG recordings. NeuroImage 59 (3), 2073–2087.

Luo, Q., Huang, X., Glover, G.H., 2014. Ballistocardiogram artifact removal with a reference layer and standard EEG cap. J. Neurosci. Methods 233, 137–149.

Maggioni, E., Arrubla, J., Warbrick, T., Dammers, J., Bianchi, A.M., Reni, G., Tosetti, M., Neuner, I., Shah, N.J., 2014. Removal of pulse artefact from EEG data recorded in MR environment at 3 T. Setting of ICA parameters for marking artefactual components: application to resting-state data. PLoS ONE 9, e112147.

Mantini, D., Perrucci, M.G., Del Gratta, C., Romani, G.L., Corbetta, M., 2007. Electrophysiological signatures of resting state networks in the human brain. Proc. Natl. Acad. Sci. 104, 13170–13175.

Masterton, R.A.J., Abbott, D.F., Fleming, S.W., Jackson, G.D., 2007. Measurement and reduction of motion and ballistocardiogram artefacts from simultaneous EEG and fMRI recordings. NeuroImage 37, 202–211.

Moosmann, M., Schönfelder, V.H., Specht, K., Scheeringa, R., Nordby, H., Hugdahl, K., 2009. Realignment parameter-informed artefact correction for simultaneous EEG-fMRI recordings. NeuroImage 45, 1144–1150.

Mugler, J.P., Brookeman, J.R., 1990. Three-dimensional magnetization-prepared rapid gradient-echo imaging (3D MP RAGE). Magn. Reson. Med. 15, 152–157.

Negishi, M., Abildgaard, M., Laufer, I., Nixon, T., Constable, R., 2008. An EEG (electroencephalogram) recording system with carbon wire electrodes for simultaneous EEG-fMRI (functional magnetic resonance imaging) recording. J. Neurosci. Methods 173, 99–107.

Niazy, R.K., Beckmann, C.F., Iannetti, G.D., Brady, J.M., Smith, S.M., 2005. Removal of FMRI environment artifacts from EEG data using optimal basis sets. NeuroImage 28, 720–737.

Nierhaus, T., Gundlach, C., Goltz, D., Thiel, S., Pleger, B., Villringer, A., 2013. Internal ventilation system of MR scanners induces specific EEG artifact during simultaneous EEG-fMRI. NeuroImage 74, 70–76.

Oostenveld, R., Fries, P., Maris, E., Schoffelen, J.M., 2011. FieldTrip: open source software for advanced analysis of MEG, EEG, and invasive electrophysiological data. Comput. Intell. Neurosci. 2011, 1.

Ritter, P., Becker, R., Graefe, C., Villringer, A., 2007. Evaluating gradient artifact correction of EEG data acquired simultaneously with fMRI. Magn. Reson. Imaging 25, 923–932.

Rosa, M.J., Daunizeau, J., Friston, K.J., 2010. EEG-fMRI integration: a critical review of biophysical modeling and data analysis approaches. J. Integr. Neurosci. 09, 453–476.

Thornton, R., Laufs, H., Rodionov, R., Cannadathu, S., Carmichael, D.W., Vulliemoz, S., Salek-Haddadi, A., McEvoy, A.W., Smith, S.M., Lhatoo, S., 2010. EEG correlated functional MRI and postoperative outcome in focal epilepsy. J. Neurol. Neurosurg. Psychiatry 81 (8), 922–927.

Vanderperren, K., De Vos, M., Ramautar, J.R., Novitskiy, N., Mennes, M., Assecondi, S., Vanrumste, B., Stiers, P., Van den Bergh, B.R., Wagemans, J., Lagae, L., Sunaert, S., Van Huffel, S., 2010. Removal of BCG artifacts from EEG recordings inside the MR scanner: a comparison of methodological and validation-related aspects. Neuroimage 50 (3), 920–934.

van der Meer, J.N., Pampel, A., van Someren, E.J.W., Ramautar, J.R., van der Werf, Y.D., Gomez-Herrero, German, Lepsien, J., Hellrung, L., Hinrichs, H., Möller, H.E., Walter, M., 2015n. "Eyes Open–Eyes Closed" EEG/fMRI Data Set for Evaluating Hardware Motion Sensors (Carbon-Wire Loops) with Respect to Correction of the Helium Pump Artefact. Data in Brief [Submitted for publication].

Van Houdt, P.J., de Munck, J.C., Zijlmans, M., Huiskamp, G., Leijten, F.S.S., Boon, P.A.J.M., Ossenblok, P.P.W., 2010. Comparison of analytical strategies for EEG-correlated fMRI data in patients with epilepsy. Magn. Reson. Imaging 28, 1078–1086.

Van Houdt, P.J., Ossenblok, P.P.W., Colon, A.J., Boon, P.A.J.M., de Munck, J.C., 2012. A framework to integrate EEG-correlated fMRI and intracerebral recordings. NeuroImage 60, 2042–2053.

Zotev, V., Krueger, F., Phillips, R., Alvarez, R.P., Simmons, W.K., Bellgowan, P., Drevets, W.C., Bodurka, J., 2011. Self-regulation of amygdala activation using real-time fMRI neurofeedback. PLoS ONE 6, e24522.

Zotev, V., Phillips, R., Yuan, H., Misaki, M., Bodurka, J., 2014. Self-regulation of human brain activity using simultaneous real-time fMRI and EEG neurofeedback. NeuroImage 85 (3), 985–995.